1 **Quantifying rates of cell migration and cell proliferation in co-culture**

2 **barrier assays reveals how skin and melanoma cells interact during**

3 **melanoma spreading and invasion.**

4 Parvathi Haridas [a,b,*], Catherine J. Penington [b,*], Jacqui A. McGovern [a], D. L. Sean McElwain

5 [a, b], Matthew J. Simpson [a,b,†]

6 [a] *Institute of Health and Biomedical Innovation, Queensland University of Technology (QUT), Kelvin*

7 *Grove 4059, Australia.*

8 [b] *School of Mathematical Sciences, QUT, PO Box 2434, Brisbane 4001, Australia.*

9 [*]These authors contributed equally to this work.

10 [†]Corresponding author matthew.simpson@qut.edu.au

## ABSTRACT

Malignant spreading involves the migration of cancer cells amongst other native cell types. For example, *in vivo* melanoma invasion involves individual melanoma cells migrating through native skin, which is composed of several distinct subpopulations of cells. Here, we aim to quantify how interactions between melanoma and fibroblast cells affect the collective spreading of a heterogeneous population of these cells *in vitro*. We perform a suite of circular barrier assays that includes: (i) monoculture assays with fibroblast cells; (ii) monoculture assays with SK-MEL-28 melanoma cells; and (iii) a series of co-culture assays initiated with three different ratios of SK-MEL-28 melanoma cells and fibroblast cells. Using immunostaining, detailed cell density histograms are constructed to illustrate how the two subpopulations of cells are spatially arranged within the spreading heterogeneous population. Calibrating the solution of a continuum partial differential equation to the experimental results from the monoculture assays allows us to estimate the cell diffusivity and the cell proliferation rate for the melanoma and the fibroblast cells, separately. Using the parameter estimates from the monoculture assays, we then make a prediction of the spatial spreading in the co-culture assays. Results show that the parameter estimates obtained from the monoculture assays lead to a reasonably accurate prediction of the spatial arrangement of the two subpopulations in the co-culture assays. Overall, the spatial pattern of spreading of the melanoma cells and the fibroblast cells is very similar in monoculture and co-culture conditions. Therefore, we find no clear evidence of any interactions other than cell-to-cell contact and crowding effects.

## KEYWORDS

Cell migration; Cell proliferation; Melanoma; Fibroblast; Cancer.

## 1. Introduction

Melanoma is the deadliest form of skin cancer and arises due to the malignant transformation of melanocytes (Geller and Annas, 2003). In Australia, melanoma is reported to be the third most common cancer (Melanoma Institute Australia, 2016), and it is associated with high rates of mortality (Sneyd et al., 2013). However, if melanoma is detected early, before significant spreading occurs, prognosis after surgery is very good (Erdei et al., 2010; Faries and Ariyan, 2011). Therefore, understanding the mechanisms that drive melanoma spreading and invasion is very important.

Melanoma spreading takes place in a complex environment that including the extracellular matrix and many different kinds of cell types including: endothelial cells; keratinocytes; fibroblasts and immune cells (Cornil et al., 1991; Flach et al., 2011). Melanoma spreading in the dermis involves the movement of individual melanoma cells through an environment that also contains fibroblast cells (Li et al., 2007; Sriram et al., 2015). Previous experimental work suggests that melanoma cells can interact with fibroblast cells through diffusible factors, such as growth factors and cytokines, or by cell-to-cell contact and crowding (Flach et al., 2011; Goldstein et al., 2005; Labrousse et al., 2004; Ruiter et al., 2002; Zhou et al., 2015). In the experimental literature, these kinds of interactions are often broadly referred to as *cross-talk* between different subpopulations (Dvorankova et al., 2016; Ye et al., 2014). Although experimental studies indicate that fibroblasts can play a role in cancer progression, the precise details of how melanoma cells and fibroblast cells interact are not well understood (Kalluri and Zeisberg, 2006; Li et al., 2003).

56    Metastatic melanoma cells are known to grow in colonies, that are sometimes called nests

57    (Baraldi et al., 2013; Schwartz et al., 2008). The spatial expansion of these colonies is driven

58    by the rate at which individual melanoma cells move, and the rate at which individual

59    melanoma cells proliferate. Therefore, to understand how quickly a population of melanoma

60    cells spreads through the surrounding environment, it is important to develop techniques that

61    allow us to quantify the rates of cell migration and cell proliferation (Treloar et al., 2013).

62    Previous *in vitro* studies examining the spatial spreading of populations of melanoma cells have

63    focused on monoculture experiments that contain only melanoma cells (Cornil et al., 1991; Im

64    et al, 2012; Justus et al., 2014; Treloar et al., 2013). To make these kinds of *in vitro* studies

65    more relevant to the *in vivo* environment, it is important to investigate, and quantify, how the

66    spatial spreading of melanoma cells is affected by interactions with other cells types, such as

67    fibroblasts.

68

69    In this study we perform a series of monoculture and co-culture barrier assays to examine the

70    spatial and temporal patterns of the spreading of a heterogeneous cell population that is

71    composed of both melanoma cells and primary fibroblast cells. All experiments in this work

72    make use of the human metastatic melanoma cell line SK-MEL-28 (Fofaria and Srivastava,

73    2014), whereas the fibroblast cells are primary cells obtained from human donors. We first

74    examine the spreading of melanoma cells and primary fibroblast cells separately, in a series of

75    monoculture experiments. This allows us to quantify the rate of cell proliferation and the cell

76    diffusivity for both melanoma cells and primary fibroblast cells, separately. Then, using our

77    estimates of:

78

79

80    (i)    the melanoma cell diffusivity;

81    (ii)    the primary fibroblast cell diffusivity;

82    (iii)    the melanoma cell proliferation rate; and,

83    (iv)    the primary fibroblast cell proliferation rate,

84

85    we investigate whether the solution of an appropriate mathematical model describing the co-

86    culture experiments, parameterised using data from the monoculture experiments, is able to

87    predict the patterns of spreading in a suite of co-culture experiments where both cell types are

88    present in varying ratios. The procedure that we describe can be used to quantify the extent to

89    which the interactions between the two cell types affect the co-culture experiments.

90    In summary, we present a method that can be used to identify potential interactions between

91    two different cell types. In particular, we focus on interactions between primary fibroblast cells

92    and SK-MEL-28 melanoma cells. Our hypothesis is that the rates at which these cells

93    proliferate and migrate might be different when the cells are cultured in isolation to when the

94    cells are cultured together. Overall, the results of our experimental and mathematical study

95    supports the null hypothesis, since we find no clear evidence of any interactions other than cell-

96    to-cell contact and crowding effects.

97

98    **2.  Experimental Methods**

99

100    *2.1  Melanoma Cell Culture*

101

5

102   The metastatic melanoma cell line, SK-MEL-28, is cultured as described previously (Haridas

103   et al., 2016). In brief, SK-MEL-28 melanoma cells are maintained in RPMI1640 medium

104   (Thermo Scientific, Australia) supplemented with 10% fetal calf serum (FCS; Thermo

105   Scientific), 2 mM L-glutamine (Thermo Scientific), 23 mM HEPES (Thermo Scientific),

106   50 U/ml of penicillin and 50 μg/ml of streptomycin (Thermo Scientific). The melanoma cell

107   line is grown at 37 °C, in 5% $CO_2$ and 95% air, and the cell line is routinely screened for

108   *mycoplasma* contamination.

109

110   *2.2 Primary fibroblast culture*

111

112   Human skin discards are obtained from abdominoplasty and breast reduction surgeries (Xie et

113   al., 2010). The epidermis is removed, discarded and the remaining dermis is used for fibroblast

114   isolation. All experimental procedures are approved by the QUT research ethics committee

115   (approval number QUT HREC #1300000063) and St Andrew's Hospital ethics committee

116   (approval number: Uniting Care Health 2003/46). The dermis is finely minced with a scalpel

117   blade and placed in a 0.05% w/v collagenase A type I (Thermo Scientific) solution prepared in

118   Dulbecco's Modified Eagle's Medium (DMEM) (Thermo Scientific) at 37 °C, in 5% $CO_2$ and

119   95% air for 24 hours. The dermal cell solution is centrifuged at 212 g for 10 minutes, and cells

120   are seeded into T75 cm² flasks (Nunc®, Australia) in DMEM with 10% FCS, 2 mM L-

121   glutamine, 50 U/ml of penicillin and 50 μg/ml of streptomycin at 37 °C in 5% $CO_2$ and 95%

122   air.

123

124   *2.3 Circular barrier assay*

6

125

126    The spreading and proliferation of both primary fibroblast cells and SK-MEL-28 melanoma

127    cells are examined using a two-dimensional circular barrier assay (Treloar et al., 2014a; Treloar

128    et al. 2014b).   Two types of experiments are performed.   Firstly, in the monoculture

129    experiments, the barrier assays are initialised with approximately 20,000 primary fibroblast

130    cells (Fb monoculture), or approximately 20,000 SK-MEL-28 melanoma cells (SK

131    monoculture).  Secondly, in the co-culture experiments, assays are performed using three ratios

132    of melanoma to fibroblast cells with the total number of initial cells held constant at

133    approximately 20,000. We use three different ratios, and refer to these experiments as: co-

134    culture 1; co-culture 2; and co-culture 3. Co-culture 1 experiments are initialised with

135    approximately 15,000 primary fibroblast cells and approximately 5,000 SK-MEL-28

136    melanoma cells; co-culture 2 experiments are initialised with approximately 10,000 primary

137    fibroblast cells and  approximately 10,000 SK-MEL-28 melanoma cells; and, co-culture 3

138    experiments are initialised with approximately 5,000 primary fibroblast cells and

139    approximately 15,000 SK-MEL-28 melanoma cells. We note that all experiments are initialised

140    with approximately 20,000 cells in total.  This means that the initial density of cells is less than

141    half of the carrying capacity density, and this allows the cell populations to spread as a

142    monolayer (Treloar et al. 2013; Treloar et al. 2014a) instead of piling up to form three-

143    dimensional structures.

144

145    Clean and dried metal-silicone barriers, 6 mm in diameter (Aix Scientifics, Germany), are

146    placed in a 24 well tissue culture plate (Nunc®) over glass coverslips (ProSciTech, Australia)

147    containing 500 μl of full Green's medium. The medium is made up of DMEM with Ham's F12

148    medium (Thermo Scientific) in a 3:1 v/v ratio, 10% FCS, 2 mM L-glutamine, 50 U/ml of

149 penicillin, 50 µg/ml of streptomycin, 180 mM adenine (Sigma Aldrich, Australia), 1 µg/ml

150 insulin, 0.1 µg/ml cholera toxin (Sigma Aldrich), 0.01% non-essential amino acid solution

151 (Thermo Scientific), 5 µg/ml transferrin (Sigma Aldrich), 0.2 µM triiodothyronine (Sigma

152 Aldrich), 0.4 µg/ml hydrocortisone (Sigma Aldrich) and 10 ng/ml human recombinant

153 epidermal growth factor (EGF; Thermo Scientific). The cell suspension is carefully pipetted

154 into the barrier to ensure the cells are as evenly distributed as possible. Cells are allowed to

155 attach to the plate for 2 hours in a humidified incubator at 37°C, 5% $CO_2$ and 95% air, before

156 the barriers are carefully removed (Treloar et al., 2013). The cell layer is washed with serum

157 free medium (SFM; culture medium without FCS) and the cells are cultured in full Green's

158 medium. The culture plates are incubated at 37°C, 5% $CO_2$ and 95% air for $t$=0, 24 and 48

159 hours. Each assay is performed in triplicates. Each assay is also repeated using primary

160 fibroblast cells from three separate human donors.

161

162 *2.4 Crystal violet staining*

163

164 The cells grown on coverslips are washed with phosphate buffered saline (PBS; Thermo

165 Scientific) and fixed for 20 minutes at room temperature using 10% neutral buffered formalin

166 (United Biosciences, Australia), followed by staining the cells in 0.01% v/v crystal violet

167 (Sigma Aldrich) in PBS. The coverslips are rinsed with PBS to remove excess stain and are

168 air-dried. Images of the entire spreading cell population are acquired using a stereo microscope

169 (Nikon SMZ 800) fitted with a Nikon digital camera.

170

171 *2.5 Immunofluorescence*

172

173    Cells grown on coverslips are fixed with 4% paraformaldehyde (Electron Microscopy

174    Sciences, Australia) for 20 minutes at room temperature. Cell membranes are permeabilised

175    with 0.1% v/v Triton X-100 (Merck Millipore, Australia) in PBS for 10 minutes, and the non-

176    specific binding sites are blocked using 0.5% w/v bovine serum albumin (BSA) (Thermo

177    Scientific) in PBS for 10 minutes. This is followed by the addition of primary antibody, *S100*

178    in a ratio of 1:2000 (Dako, Australia) for an hour, and the secondary antibody *Alexa Fluor*[®]

179    555 in a ratio of 1:400 (Thermo Scientific) for an hour. Cells are washed with 0.5% BSA and

180    the nuclei are stained with *dapi* in a ratio of 1:1000 (Sigma Aldrich) for 5 minutes. Coverslips

181    are mounted on glass slides using ProLong[®] Gold Antifade mountant (Thermo Scientific).

182

183    **3. Mathematical modelling methods**

184

185    *3.1 Model summary*

186

187    One way of providing further information about cancer progression is to interpret experimental

188    observations using a mathematical model (Byrne, 2010). To quantify the role of various

189    mechanisms acting in the monoculture and co-culture experiments we will use a continuum

190    partial differential equation (PDE) model describing the collective spreading, proliferation and

191    cell-to-cell crowding in a heterogeneous population of cells that is composed of two distinct

192    subpopulations (Simpson et al. 2014). The PDE model is given by,

$$\frac{\partial C_{Fb}}{\partial t} = \frac{D_{Fb}}{r} \frac{\partial}{\partial r}\left(r\left[\left[1-\frac{S}{K}\right]\frac{\partial C_{Fb}}{\partial r} + \frac{C_{Fb}}{K}\frac{\partial S}{\partial r}\right]\right) + \lambda_{Fb}C_{Fb}\left(1-\frac{S}{K}\right), \tag{1}$$

$$\frac{\partial C_{SK}}{\partial t} = \frac{D_{SK}}{r} \frac{\partial}{\partial r}\left(r\left[\left[1-\frac{S}{K}\right]\frac{\partial C_{SK}}{\partial r} + \frac{C_{SK}}{K}\frac{\partial S}{\partial r}\right]\right) + \lambda_{SK}C_{SK}\left(1-\frac{S}{K}\right), \tag{2}$$

193   where $C_{Fb}(r,t)$ and $C_{SK}(r,t)$ are the density of fibroblast and melanoma cells, respectively,

194   as a function of radial position, $r$, and time, $t$. The total cell density is given by

195   $S(r,t) = C_{Fb}(r,t) + C_{SK}(r,t)$, and the carrying capacity density is $K$. Since we consider

196   circular barrier assays, in which the population of spreading cells always maintains a circular

197   geometry over the entire duration of the experiment, Eq. (1)-(2) are written in terms of the

198   radial coordinate, $r$, taking advantage of the axisymmetric geometry. Note that if there is just

199   a single population present, Eq. (1)-(2) reduces to the standard Fisher-Kolmogorov equation in

200   radial geometry (Treloar et al. 2014a).

201

202   *3.2 Model parameters*

203

204   There are five parameters in the co-culture model: (i) $D_{Fb}$ is the diffusivity of the primary

205   fibroblast cells; (ii) $D_{SK}$ is the diffusivity of the SK-MEL-28 melanoma cells; (iii) $\lambda_{Fb}$ is the

206   proliferation rate of the primary fibroblast cells; (iv) $\lambda_{SK}$ is the proliferation rate of the SK-

207   MEL-28 melanoma cells; and (v) $K$ is the carrying capacity density. Since the cells in our

208   experiments spread as a monolayer, and the diameter of both the primary fibroblast cells and

209   the SK-MEL-28 melanoma cells is approximately 20 μm (Treloar et al. 2013; Treloar et al.

210   2014a), we estimate the carrying capacity density by assuming that the maximum density of

211   cells corresponds to hexagonal packing of disks of diameter 20 μm, giving $K = 2.8 \times 10^{-3}$

212   cells/μm². With this assumption there are now four unknown parameters in Eq. (1)-(2).

213

214   *3.3 Initial condition*

215

216   The PDE model can be used to simulate both co-culture and a monoculture barrier assays. To

217   simulate a co-culture assay we specify appropriate non-zero initial conditions for both

218   $C_{Fb}(r,0)$ and $C_{SK}(r,0)$, chosen to match the initial cell density in the co-culture experiments.

219   Alternatively, to simulate a fibroblast monoculture assay, we set $C_{SK}(r,0) = 0$ and specify

220   some appropriate non-zero initial condition for $C_{Fb}(r,0)$. Similarly, to simulate a melanoma

221   monoculture assay we set $C_{Fb}(r,0) = 0$ and specify some appropriate non-zero initial condition

222   for $C_{SK}(r,0)$.

223

224   *3.4 Numerical solution*

225

226   Regardless of whether we use the PDE model to simulate a monoculture or co-culture assay,

227   we always solve Eq.(1)-(2) numerically. Spatial derivatives are approximated using a central

228   difference approximation on a uniformly-spaced finite difference mesh, with mesh spacing $\Delta r$

229   . The resulting system of coupled nonlinear ordinary differential equations is solved using a

230   backward Euler approximation, with time steps of duration $\Delta t$. The nonlinear ordinary

231   differential equations are linearised using Picard iteration with a convergence tolerance of $\varepsilon$

232   (Chapra and Canale, 1998).

233

234   *3.5 Model background*

11

235

236    Before applying Eq. (1)-(2) to our experimental data set, it is useful to briefly explain the origin

237    of the PDE model and the underlying assumptions. The model was described and presented

238    by us previously (Simpson et al. 2014). In that previous work we consider both a stochastic

239    random walk process and the associated continuum limit PDE description. In brief, the lattice

240    based random walk model describes the collective motion of a population of two potentially

241    distinct subpopulations of cells. Cells in both subpopulations undergo nearest neighbour

242    motility events, where cells attempt to step a distance of $\Delta$, at some specified constant rate.

243    Here, $\Delta$ corresponds to the average cell diameter. Potential motility events are unbiased so that

244    the direction of movement is chosen with equal probability. Crowding effects are incorporated

245    by ensuring that any potential motility event that would place a cell on an occupied site is

246    aborted. The discrete model also allows cells to proliferate, at some other specified constant

247    rate. A potential proliferation event will involve a cell placing a daughter cell, of the same

248    subpopulation, on a randomly chosen nearest neighbour lattice site. Again, crowding effects

249    are incorporated by ensuring that any potential proliferation event that would place a daughter

250    cell on an occupied lattice site is aborted. The continuum limit description of this discrete

251    model, in a radially symmetric geometry, is Eq. (1)-(2) (Simpson et al., 2014).

252

253    The system of PDEs, given by Eq. (1)-(2), corresponds to a coarse-grained description of the

254    cell-to-cell crowding effects that are explicitly described in the discrete random walk model.

255    For example, the nonlinear diffusion terms in Eq. (1)-(2) correspond to hard-core exclusion in

256    the motility mechanism of the discrete model. Similarly, the nonlinear source terms in Eq. (1)-

257    (2) correspond to the proliferation mechanism of the discrete model.

258

## 4. Experimental results and discussion

*4.1 Diameter of the spreading population*

We first investigate the spatial expansion of the cell populations over time. Results in Fig. 1(a)-(i) show the spreading populations from $t=0$ until $t=48$ hours. To quantify the spatial spreading, we calculate the diameter of each spreading population at $t=0$, 24 and 48 hours. To achieve this we use ImageJ (2016) to automatically detect the position of the leading edge of the spreading population using the Sobel method (Treloar and Simpson, 2013; Johnston et al. 2014). ImageJ also provides an estimate of the area contained within the leading edge of the spreading population. Using this estimate of area, we assume that the spreading population remains approximately circular, allowing us to convert the area estimate into an estimate of the equivalent circular diameter. The diameter of the spreading populations is shown in Fig. 1(j) where we see that there is an increase in the diameter with time in all cases. However, we observe that the rate of increase in the diameter in some experiments is different. For example, we observe that Fb monoculture experiments spread fastest, whereas the SK monoculture experiments spread slowest. In comparison, the co-culture experiments spread at an intermediate rate.

Although these results focusing on the rate at which the leading edge of the populations spread is insightful, they do not provide any information about how the primary fibroblast cells and the SK-MEL-28 melanoma cells are distributed throughout the spreading populations. To provide this additional information, we use a more sophisticated experimental approach.

282     *4.2 Cell type identification in co-cultures*

283

284     To extend our initial investigation about the spatial expansion of the cell populations, we

285     quantify the spatial distribution of primary fibroblast cells and SK-MEL-28 melanoma cells

286     throughout the spreading populations. To achieve this we must distinguish the primary

287     fibroblast cells from the SK-MEL-28 melanoma cells within these heterogeneous populations.

288     The metastatic melanoma cell line, SK-MEL-28 can be reliably and exclusively identified

289     using the *S100* marker (Haridas et al., 2016). However, it is challenging to identify primary

290     fibroblast cells in a heterogeneous population because many because fibroblast markers, like

291     *vimentin* and *alpha smooth muscle actin*, are also expressed by other migrating cell types

292     present in the population (Kalluri and Zeisberg, 2006; Marsh et al., 2013; Sugimoto et al.,

293     2006). To deal with this complication we use *dapi* to stain the cell nuclei of all cells, capturing

294     both the SK-MEL-28 melanoma cells and the primary fibroblast cells.  By counting the number

295     of *dapi*-positive cells and subtracting the number of *S100* positive cells, we are able to reliably

296     estimate the number of primary fibroblast cells in each image.

297

298     Images showing the entire spreading populations are superimposed with an immunostained

299     transect that passes through the centre of the cell population in Fig. 2. These immunostained

300     transects allow us to extract detailed information about the spatial distribution of primary

301     fibroblast cells and SK-MEL-28 melanoma cells in each experiment. Greyscale images

302     showing the entire spreading population at $t$=24 and 48 hours are shown in Fig. 2(a), (c), (e),

303     (g), (i), (k), (m), (o), (q) and (s). The central region of the transect, as indicated, is magnified

304     and shown in Fig. 2(b), (d), (f), (h), (j), (l), (n), (p), (r) and (t). Our results in Fig. 2 show that

305     we are able to clearly and reliably identify the two different cell types in the experiments. We

14

306    are confident in our results because there are no *S100* positive cells in the primary fibroblast

307    monoculture experiment (Fig. 2(b), (d)), and we observe an increasing proportion of *S100*

308    positive cells in co-culture 3 (Fig. 2(m)-(p)), compared to co-culture 2 (Fig. 2(i)-(l)). Similarly,

309    we observe an increasing proportion of *S100* positive cells in co-culture 2 (Fig. 2(i)-(l)),

310    compared to co-culture 1 (Fig. 2(e)-(h)).

311

312    *4.3 Construction of cell density histograms*

313

314    To quantify how the two subpopulations of cells are spatially distributed within the

315    heterogeneous spreading populations, we construct cell density histograms. To do this, we

316    count the number of cells in many equally spaced subregions across each transect, as shown in

317    Fig. 3(a). We use immunofluorescence to identify primary fibroblast cells and SK-MEL-28

318    melanoma cells as described in Section *4.2*, and as shown in Fig. 3(b)-(d). An estimate of the

319    cell density for each cell type along the transect is calculated by counting the number of primary

320    fibroblast cells and the number of SK-MEL-28 melanoma cells in each subregion, and dividing

321    these numbers by the area of the subregion. A histogram showing cell density as a function of

322    position is generated for each experimental replicate in each experimental condition.

323    Averaging the histograms from each experimental replicate gives an averaged histogram, as

324    shown in Fig. 3(e). The raw data showing the cell density information for each experimental

325    replicate is also provided (Supplementary Material-1).

326

327    A series of averaged cell density histograms at $t$=0, 24 and 48 hours are shown in Fig. 4. Each

328    histogram shows the average density of cells across the entire transect. The radial position is

15

329    given by $r>0$. The centre of the spreading cell population corresponds to $r=0$, and the

330    population spreads in both directions, away from the centre. The blue section in the histograms

331    indicate the average density of primary fibroblast cells, the red section shows the average

332    density of SK-MEL-28 melanoma cells, and the total height of the histogram shows the average

333    total cell density.

334

335    Results in Fig. 4(a), (d), (g), (j) and (m) show the histograms at $t=0$. These results confirm that

336    all barrier assays are initialised such that the total population of cells is approximately

337    uniformly distributed across the transect, with a total cell density of approximately

338    $1\times10^{-3}$ cells/$\mu m^2$, which is less than half the carrying capacity density of these cells in a

339    monolayer (Supplementary Material-2). However, the ratio of melanoma to primary fibroblast

340    cells differs in Fig. 4(a), (d), (g), (j) and (m). For example, the profile in Fig. 4(a) contains only

341    primary fibroblast cells, the prolife in Fig. 4(m) contains only melanoma cells, and the profiles

342    in Fig. 4(d), (g) and (j) contain both melanoma and primary fibroblast cells with an increasing

343    ratio of melanoma to fibroblast cells, respectively.

344

345    Our results in each row in Fig. 4 show how the cell density changes with time. The middle

346    column of results corresponds to $t=24$ hours, and the right-most column corresponds to $t=48$

347    hours. Comparing results in Fig. 4(c) and Fig. 4(o) shows that the cells in the Fb monoculture

348    experiments spread further than the cells in the SK monoculture experiments, and result this is

349    consistent with the leading edge results in Fig. 1. Furthermore, comparing the shape of the cell

350    density histograms in Fig. 4(c) and Fig. 4(o) shows that the leading edge of the cell density

351    profile is sharper in the SK monoculture experiments than for the Fb monoculture experiments.

352    While we observe differences in the rate of the spatial extent of the spreading of the two

16

353    monoculture experiments, we observe that the increase in cell density towards the centre of the

354    population, at $r$=0, is very similar. For example, at $t$=0 the cell density at the centre of both

355    monoculture experiments is approximately $1\times10^{-3}$ cells/$\mu$m$^2$, and after 48 hours the cell density

356    at the centre of both monoculture experiments has approximately doubled to a density of

357    $2\times10^{-3}$-$2.5\times10^{-3}$cells/$\mu$m$^2$.

358

359    Comparing the time evolution of the cell density patterns in the co-culture experiments with

360    the monoculture experiments suggests that there are minimal differences in the behaviour of

361    the monoculture and co-culture experiments. For example, co-culture 1 that is initiated with

362    approximately 15,000 primary fibroblast cells and approximately 5,000 SK-MEL-28

363    melanoma cells behaves in a very similar way to the Fb monoculture experiment in terms of

364    both the spatial extent of the spreading of the total population and the total increase in the cell

365    density towards the centre of the spreading population. Similarly, co-culture 3, that is initiated

366    with approximately 5,000 primary fibroblast cells and approximately 15,000 SK-MEL-28

367    melanoma cells behaves in a very similar way unto the SK monoculture experiment in terms

368    of both the spatial extent of the spreading of the total population and the total increase in the

369    cell density towards the centre of the spreading population. Results for co-culture 2 lie between

370    co-culture 1 and co-culture 3. An interesting feature of co-culture 1 and co-culture 2 is that at

371    both $t$=24 and $t$=48 hours, we see that the primary fibroblast cells dominate the total population

372    right at the leading edge of the heterogeneous population of cells. This is consistent with our

373    observation that the primary fibroblast cells spread faster than the SK-MEL-28 melanoma cells

374    in the monoculture experiments.

375

17

376    Now that we have presented, and discussed, the cell density histograms for the monoculture

377    and co-culture experiments, we will further explore the similarities and differences between

378    the experiments by calibrating a mathematical model to these data. Combining our

379    experimental results with a mathematical model will allow us to explore, in more detail, the

380    question of whether the primary fibroblast cells and/or the SK-MEL-28 melanoma cells behave

381    differently when grown in monoculture or in co-culture conditions.

382

383    **5. Mathematical results and discussion**

384

385    *5.1 Estimating parameters for the monoculture experiments*

386

387    Since fibroblast cells and melanoma cells are cultured separately in the monoculture

388    experiments, the coupled model, given by Eq. (1)-(2), uncouples to give

$$\frac{\partial C_{Fb}}{\partial t} = \frac{D_{Fb}}{r}\frac{\partial}{\partial r}\left(r\frac{\partial C_{Fb}}{\partial r}\right) + \lambda_{Fb}C_{Fb}\left(1 - \frac{C_{Fb}}{K}\right), \tag{3}$$

$$\frac{\partial C_{SK}}{\partial t} = \frac{D_{SK}}{r}\frac{\partial}{\partial r}\left(r\frac{\partial C_{SK}}{\partial r}\right) + \lambda_{SK}C_{SK}\left(1 - \frac{C_{SK}}{K}\right). \tag{4}$$

389    Equations (3)-(4) are two, uncoupled, single-species Fisher-Kolmogorov equations in radial

390    coordinates that we will use to describe the Fb monoculture and SK monoculture experiments,

391    respectively. There are four parameters to be estimated: $D_{Fb}$; $D_{SK}$; $\lambda_{Fb}$ and $\lambda_{SK}$. We now

392    explain how these parameters can be estimated separately, using data in Fig. 4(a)-(c) for the Fb

393    monoculture experiment, and using data in Fig. 4(m)-(o) for the SK monoculture experiment.

394    Following the approach of Johnston et al. (2015), we note that in the central region of the

395    monoculture experiments, where $r < 1425\,\mu$m, the cell density profile is approximately

396    spatially uniform in both the fibroblast monoculture and the melanoma monoculture (Fig. 4).

397    This region approximately corresponds to the middle third of the spreading population, and

398    hence this region is well away from the leading edge of the spreading populations. Since,

399    locally in the centre of the fibroblast monoculture experiment we have $\partial C_{Fb}/\partial r \approx 0$, and

400    locally in the centre of the melanoma monoculture experiment we have $\partial C_{SK}/\partial r \approx 0$, the two

401    uncoupled PDEs, Eq. (3)-(4), simplify to two uncoupled ordinary differential equations (ODE)

402    that can be written as

$$\frac{dC_{Fb}}{dt} = \lambda_{Fb}C_{Fb}\left(1 - \frac{C_{Fb}}{K}\right), \tag{5}$$

$$\frac{dC_{SK}}{dt} = \lambda_{SK}C_{SK}\left(1 - \frac{C_{SK}}{K}\right). \tag{6}$$

403    The solutions of Eq. (5)-(6) are

$$C_{Fb}(t) = \frac{KC_{Fb}(0)\exp(\lambda_{Fb}t)}{K + C_{Fb}(0)[\exp(\lambda_{Fb}t)-1]}, \tag{7}$$

$$C_{SK}(t) = \frac{KC_{SK}(0)\exp(\lambda_{SK}t)}{K + C_{SK}(0)[\exp(\lambda_{SK}t)-1]}, \tag{8}$$

404    where $C_{Fb}(0)$ is the initial density of the fibroblast cells in the central region of the Fb

405    monoculture experiments, and $C_{SK}(0)$ is the initial density of the melanoma cells in the central

406    region of the SK monoculture experiments. Estimates of $\lambda_{Fb}$ and $\lambda_{SK}$ are obtained by choosing

407    these parameters so that $C_{Fb}(t)$ and $C_{SK}(t)$, given by Eq. (7)-(8), match the experimental data

408    from the central region of the fibroblast monoculture experiments and the melanoma

409    monoculture experiments, respectively (Supplementary Material-2). In summary, matching

410    these solutions to our experimental data gives us a range of estimates: $0.02 \leq \bar{\lambda}_{Fb} \leq 0.04$ /hour

411    and $0.03 \leq \bar{\lambda}_{SK} \leq 0.05$ /hour. Here we use the overbar notation to indicate the least-squares

412    estimates of the parameters, and the range of estimates corresponds to the sample mean plus or

413    minus one sample standard deviation calculated using the three identically prepared

414    experimental replicates of the monoculture experiments. It is interesting to note that these

415    estimates of the proliferation rate for the melanoma cells and the fibroblast cells are

416    approximately equal. Furthermore, the proliferation rates correspond to a doubling time of

417    approximately 23 hours, and this is consistent with previous results (Treloar et al. 2013).

418

419    Given our estimates of $\lambda_{Fb}$ and $\lambda_{SK}$, we solve Eq. (3)-(4) across the entire domain, $0 < r < 4350$

420    µm, and match the numerical solution of each uncoupled PDE with the averaged cell density

421    profiles across the entire domain for both monoculture experiments. Setting the proliferation

422    rates to be in the middle of the range previously identified ($\bar{\lambda}_{Fb} = 0.03$/hour and $\bar{\lambda}_{SK} = 0.04$

423    /hour), we obtain estimates of $\bar{D}_{Fb} \approx 1200\,\mu\text{m}^2$/hour, and $\bar{D}_{SK} \approx 170\,\mu\text{m}^2$/hour

424    (Supplementary Material-2). Unlike our estimates of the proliferation rates, the estimate of the

425    cell diffusivity for the fibroblast cells is an order of magnitude higher than the estimate of the

426    cell diffusivity for the melanoma cells. Our estimate for the cell diffusivity of the human

427    primary fibroblast cells is very similar to previous estimates of the cell diffusivity for 3T3

428    mouse fibroblast cells, which have been reported to be approximately 800-2900 $\mu\text{m}^2$/hour

429    (Treloar et al. 2014a). Furthermore, our estimate of the cell diffusivity for the SK-MEL-28

430    melanoma cells is similar to previous estimates for other metastatic melanoma cell lines, which

431    have been reported to be approximately 160-250 $\mu\text{m}^2$/hour (Treloar et al. 2013).

432

433    *5.2 Predicting collective cell spreading in the co-culture experiments*

434

435    Given our parameter estimates from the monoculture experiments, we are interested to

436    investigate whether the solution of the coupled co-culture model, Eq. (1)-(2), can accurately

437    predict the spatial and temporal patterns of spreading in the co-culture experiments when

438    parameterised in the same way. Examining this question will provide insight into whether the

439    fibroblast and/or melanoma cells behave differently in monoculture than they do in co-culture.

440    In summary, if we can find a unique choice of $D_{Fb}$; $D_{SK}$; $\lambda_{Fb}$ and $\lambda_{SK}$ for which:

441

442    (i)    the solution of the coupled system, Eq. (1)-(2), matches the experimental data

443           for all three co-culture assays;

444    (ii)   the solution of Eq. (3) matches the experimental data for the fibroblast

445           monoculture assay; and

446    (iii)  the solution of Eq. (4) matches the experimental data for the melanoma

447           monoculture assay,

448

449    it would be reasonable to conclude that the migratory and proliferative behaviour of the

450    melanoma and fibroblast cells appears to be independent of whether these two cell types are

451    cultured separately or together. In contrast, if we must choose very different parameter values

452    to match the monoculture experiments compared to the parameter values required to match the

453    co-culture experiments, then our results would suggest that the cells behave very differently in

454    monoculture and co-culture environments.

455

456    Results in Fig. 5 compare the spatial and temporal evolution of the two monoculture assays

457    and the three co-culture assays together with the solution of the appropriately parameterised

21

458    mathematical models. Using our parameter estimates from the monoculture experiments as an

459    initial estimate, we manually adjusted the parameters and find that setting $D_{Fb} \approx 1200$

460    $\mu m^2$/hour; $D_{SK} \approx 170$ $\mu m^2$/hour; $\lambda_{Fb} = 0.03$/hour and $\lambda_{SK} = 0.03$/hour leads to a reasonably

461    accurate match across both the two monoculture assays and the three co-culture assays

462    (Supplementary Material-2). Given that we are able to match both the monoculture and co-

463    culture experiments using a single combination of parameters, this suggests that the only

464    interactions necessary to explain the experimental observations are cell-to-cell contact and

465    crowding effects. In particular, no additional cross-talk mechanisms, such as interactions

466    mediated by the production of signalling factors, is required to explain our experimental

467    observations.

468

469    Results in Fig. 4-5 indicate that cell density profile for co-culture 1 appears to contain a 'dip'

470    in the central region, near $r = 0$ $\mu m$. Equivalent results for co-cultures 2, 3, and the

471    monoculture experiments do not contain such a pronounced dip (Fig. 4-5). Since all

472    experiments are prepared using the same procedure, we prefer not to offer an interpretation of

473    this dip because it could be due to a statistical fluctuation rather than some underlying

474    mechanism.

475

476    All of our results, so far, suggest that the diffusivity and proliferation rate of primary fibroblast

477    cells and SK-MEL-28 melanoma cells are insensitive to whether the cell populations are grown

478    in monoculture or co-culture. This implies that there is limited interactions or crosstalk

479    between these two cell populations. If we were to observe some interactions, such as melanoma

480    cell migration being stimulated by the presence of fibroblast cells, we can use our mathematical

481      model to explore how these potential interactions might be best observed. To explore this we

482      conduct a series of numerical experiments to investigate how the solutions of Eq. (1)-(2)

483      depend on $D_{SK}$. Since we focus on altering $D_{SK}$ alone, we find that the solution of Eq. (1)-(2)

484      is most sensitive at the low-density leading edge of the population, as depicted in Fig. 6(a).

485      Results in Fig. 6(b) compare the experimental density profile for co-culture 3 at $t = 48$ hours

486      with the standard choice of parameters from Fig 5, showing that the solution of the

487      mathematical model for $S(r,t)$ matches the experimental data quite well at the leading edge

488      of the spreading population. We also show results where $D_{SK}$ is increased by a factor of 5,

489      where we see that the solution of the mathematical model predicts that the population spreads

490      notably further than observed in the experiments. Similarly, we also show equivalent results

491      where $D_{SK}$ is increased by a factor of 20 and the differences are even more pronounced.

492

493      The additional results in Fig. 6 suggest that the comparison of the experimental cell density

494      profile and the solution of the mathematical model at the leading edge of the spreading

495      population is relatively sensitive to the value of $D_{SK}$. One way of interpreting the results in

496      Fig. 6(b) is that our procedure could be used to detect potential interactions that would lead to

497      a modest increase in $D_{SK}$ when the two cell types are grown in co-culture.

498

499      **6. Conclusion**

500      Many *in vitro* studies examining the spatial spreading of cancer cells use monoculture

501      experiments (Kramer et al., 2013; Liao et al., 2013; Treloar et al., 2013; Treloar et al., 2014b).

502      However, these monoculture experiments are unrealistic in the sense that the spreading cancer

503    cells are not subject to interactions with other cell types as would occur *in vivo*. To address this

504    limitation, our approach to investigate the spatial spreading of a melanoma cell population is

505    to examine a suite of monoculture and co-culture circular barrier assays. Our monoculture

506    experiments involve studying both primary fibroblast cells and SK-MEL-28 melanoma cells

507    separately, while our co-culture experiments use three ratios of both cell types in the same

508    experiment. All of our experiments are initialised by placing approximately 20,000 cells into

509    the barrier, and we examine the collective spreading over a period of 48 hours. To quantify

510    how these heterogeneous populations of cells spread over time we: (i) measure the diameter of

511    each expanding cell population; (ii) identify individual cell types in each expanding population;

512    (iii) count the number of primary fibroblast cells and SK-MEL-28 melanoma cells in a series

513    of transects across each expanding cell population; and (iv) construct cell density histograms

514    to show the spatial arrangements of each cell type in each expanding cell population.

515

516    Previous experimental studies suggest that interactions between fibroblast and melanoma cells

517    can lead to an increase in rates of collective spreading when these two cell types are in contact

518    (Cornil et al., 1991; Flach et al., 2011). However, these previous studies do not make detailed

519    measurements of spatial and temporal arrangements of cells within the spreading population,

520    and they do not consider varying the initial ratio of fibroblast cells to melanoma cells. To

521    provide more information about the interaction between melanoma cells and fibroblast cells,

522    we perform co-culture experiments using three different initial ratios of cells, and we make

523    detailed measurements about the spatial and temporal arrangements of both subpopulations

524    within the heterogeneous population as it spreads and grows.  In summary, our experimental

525    results indicate that the influence of primary fibroblast cells on SK-MEL-28 melanoma cell

526    growth and spatial expansion in a two-dimensional circular barrier assay is minimal. To

24

527  provide additional information about this apparent lack of interaction, we also calibrate a

528  mathematical model to our experimental data.

529

530  In this work, we use our mathematical model to provide a novel analysis of experiments

531  exploring potential interactions between fibroblast cells and melanoma cells.   By first

532  estimating the cell diffusivity and cell proliferation rate for the primary fibroblast cells and SK-

533  MEL-28 melanoma cells separately in monoculture, we find that the parameter estimates are

534  consistent with previously published estimates for mouse fibroblast cells and other metastatic

535  melanoma cell lines (Treloar et al. 2013; Treloar et al. 2014a).  Therefore, we are confident in

536  our estimates of the cell diffusivity and cell proliferation rate in monocultures because they are

537  consistent with previously published data for similar experiments.   Then, to address the

538  question of whether cells in monoculture behave similarly, or differently, to cells in co-culture,

539  we investigate whether the solution of the co-culture mathematical model, parameterised using

540  estimates from the monoculture experiments, can genuinely predict the behaviour of the co-

541  culture experiments.  Since we find that a fixed choice of parameters, that is very similar to the

542  estimates from the monoculture experiments, can predict both the spatial and temporal patterns

543  of  collective  spreading  in  the  two  monoculture  experiments,  and  all  three  co-culture

544  experiments,  we  conclude  that  the  spreading  and  growth  patterns  observed  for  primary

545  fibroblast  cells  and  SK-MEL-28  melanoma  cells  are  not  affected  by  growing  them  in

546  monoculture or co-culture.

547

548  Our approach is to compare the spatial spreading of two different cell types in both monoculture

549  and co-culture circular barrier assays to quantify the rates of cell migration and the rates of cell

550  proliferation for each cell type. This approach is novel because most combined experimental

551  and mathematical modelling studies focus on monoculture experiments alone (Kramer et al.,

552  2013; Treloar et al., 2013). However, it is possible to explore other alternative experiments to

553  further extend our work. This includes performing additional experiments to examine the rates

554  of spatial spreading in different cell lines. For example, it could be of interest to repeat our

555  work using other kinds of melanoma cell lines including cell lines from earlier stages of the

556  disease, such as melanoma cells associated with the radial growth phase or the vertical growth

557  phase (Haridas et al., 2016). This could be an important consideration because our current

558  work focuses on examining potential interactions between fibroblast cells and SK-MEL-28

559  melanoma cells only. Since the SK-MEL-28 cell line is associated with the metastatic phase

560  (Fofaria and Srivastava, 2014; Haridas et al. 2016), it is possible that these cells have

561  progressed beyond being influenced by fibroblasts. Alternatively, if our experiments and

562  analysis were repeated using melanoma cells from earlier stages, it is conceivable that these

563  melanoma cells might be more responsive to the presence of fibroblasts.

564

565  Other options to extend our work might involve incorporating further types of cells to make

566  the co-culture experiments more realistic. For example, it is of interest to include both primary

567  fibroblast cells and primary keratinocyte cells in a co-culture experiment with melanoma cell

568  lines. However, this kind of extension is difficult because we would need to specifically

569  identify three different cell types to understand how the three different subpopulations are

570  spatially arranged. Therefore, we leave this extension for future consideration.

571

572

573  **Acknowledgments**

574

578 **References**

579 1. Baraldi, M. M., Alemi, A. A., Sethna, J. P., Caracciolo, S., Porta, C. A. L. M., Zapperi, S.,

580    2013. Growth and form of melanoma cell colonies. J. Stat. Mech-Theory-E. 2013, P02032.

581 2. Byrne, H. M., 2010. Dissecting cancer through mathematics: from the cell to the animal

582    model. Nat. Rev. Cancer. 10, 221-230.

583 3. Cornil, I., Theodorescu, D., Man, S., Herlyn, M., Jambrosic, J., Kerbel, R. S., 1991.

584    Fibroblast cell interactions with human melanoma cells affect tumor cell growth as a

585    function of tumor progression. P. Natl. Acad. Sci. USA. 88, 6028-6032.

586 4. Chapra, S. C., Canale, R. P., 1998. Numerical methods for engineers, third ed. McGraw-

587    Hill, Singapore.

588 5. Dvorankova, B., Szabo, P., Kodet, O., Strnad, H., Kolar, M., Lacina, L., Krejci, E., Nanka,

589    O., Sedo, A., Smetana, K. Jr., 2016. Intercellular crosstalk in human malignant melanoma.

590    Protoplasma. http://dx.doi.org/10.1007/s00709-016-1038-z (in press).

591 6. Erdei, E., Torres, S. M., 2010. A new understanding in the epidemiology of melanoma.

592    Expert Rev. Anticanc. 10, 1811-1823.

593 7. Faries, M. B., Ariyan, S., 2011. Current surgical treatment in melanoma. Curr. Prob.

594    Cancer. 35, 173-184.

595 8. Flach, E. H., Rebecca, V. W., Herlyn, M., Smalley, K. S., Anderson, A. R. A., 2011.

596    Fibroblasts contribute to melanoma tumor growth and drug resistance. Mol. Pharm. 8,

597    2039-2049.

598 9. Fofaria, N., Srivastava, S. K., 2014. Critical role of STAT3 in melanoma metastasis through

599    anoikis resistance. Oncotarget. 5, 7051-7064.

600 10. Geller, A. C., Annas, G. D., 2003. Epidemiology of melanoma and nonmelnaoma skin

601    cancer. Semin. Oncol. Nurs. 19, 2-11.

602    11. Goldstein, L. J., Chen, H., Bauer, R. J., Bauer, S. M., Velazquez, O. C., 2005. Normal

603        human fibroblasts enable melanoma cells to induce angiogenesis in type I collagen.

604        Surgery. 138, 439-449.

605    12. Haridas, P., McGovern, J. A., Kashyap, A. S., McElwain, D. L. S., Simpson, M. J., 2016.

606        Standard melanoma-associated markers do not identify the MM127 metastatic melanoma

607        cell line. Sci. Rep. 6, 24569.

608    13. Im, Y-S., Ryu, Y-K., Moon, E-Y., 2012. Mouse melanoma cell migration is dependent on

609        production of reactive oxygen species under normoxia condition. Biomol. Ther. 20, 165-

610        170.

611    14. ImageJ, ImageJ User Guide: Research Services Branch, National Institute of Health.

612        <https://imagej.nih.gov/ij/docs/guide/146-29.html> (April 2017).

613    15. Johnston, S. T., Simpson, M. J., McElwain, D. K. S., 2014. How much information can be

614        obtained from tracking the position of the leading edge in a scratch assay? J. R. Soc.

615        Interface. 11, 20140325.

616    16. Johnston, S. T., Shah, E. T., Chopin, L. K., McElwain, D. L. S., Simpson, M. J., 2015.

617        Estimating cell diffusivity and cell proliferation rate by interpreting IncuCyte ZOOM™

618        assay data using the Fisher-Komogorov model. BMC Syst. Biol. 9, 38.

619    17. Justus, C. R., Leffler, N., Ruiz-Echevarria, M., Yang, L. V., 2014. *In vitro* cell migration

620        and invasion assays. J. Vis. Exp. 88, e51046.

621    18. Kalluri, R., Ziesberg, M., 2006. Fibroblasts in cancer. Nat. Rev. Cancer. 6, 392-401.

622    19. Kramer, N., Walzl, A., Unger, C., Rosner, M., Krupitza, G., Hengstschlager, M., Dollznig,

623        H., 2013. *In vitro* cell migration and invasion assays. Mutat. Res. 752, 10-24.

624    20. Labrousse, A-L., Ntayi, C., Hornebeck, W., Bernard, P., 2004. Stromal reaction in

625        cutaneous melanoma. Crit. Rev. Oncol. Hemat. 49, 269-275.

29

626    21. Li, G., Satyamoorthy, K., Meier, F., Berking, C., Bogenrieder, T., Herlyn, M., 2003.

627        Function and regulation of melanoma-stromal fibroblast interactions: when seeds meet soil.

628        Oncogene. 22, 3162-3171.

629    22. Li, H., Fan, X., Houghton, J., 2007. Tumor microenvironment: the role of the tumor stroma

630        in cancer. J. Cell. Biochem. 101, 805-815.

631    23. Liao, S., Deng, D., Zhang, W., Hu, X., Wang, W., Wang, H., Lu, Y., Wang, S., Meng, L.,

632        Ma, D., 2013. Human papillomavirus 16/18 E5 promotes cervical cancer cell proliferation,

633        migration and invasion *in vitro* and accelerates tumor growth *in vivo.* Oncol. Rep. 29, 95-

634        102.

635    24. Marsh, T., Pietras, K., McAllister, S. S., 2013. Fibroblasts as architects of cancer

636        pathogenesis. Biochim. Biophys. Acta.1832, 1070-1078.

637    25. Melanoma Institute Australia. <https://www.melanoma.org.au/> (April 2017).

638    26. Ruiter, D., Bogenrieder, T., Elder, D., Herlyn, M., 2002. Melanoma–stroma interactions:

639        structural and functional aspects. Lancet Oncol. 3, 35-43.

640    27. Simpson, M. J., Haridas, P., McElwain, D. L. S., 2014. Do pioneer cells exist? PLoS One.

641        9, e85488.

642    28. Schwartz, M. A., McRoberts, K., Coyner, M., Andarawewa, K. L., Frierson, H. F. Jr.,

643        Sanders, J. M., Swenson, S., Markland, F., Conaway, M. R., Theodorescu, D., 2008.

644        Integrin agonists as adjuvants in chemotherapy for melanoma. Clin. Cancer Res. 14, 6193-

645        6197.

646    29. Sneyd, M. J., Cox, B., 2013. A comparison of trends in melanoma mortality in New Zealand

647        and Australia: the two countries with the highest melanoma incidence and mortality in the

648        world. BMC Cancer. 13, 372.

649    30. Sriram, G., Bigliardi, P. L., Bigliardi-Qi, M., 2015. Fibroblast heterogeneity and its
650        implications for engineering organotypic skin models *in vitro*. Eur. J. Cell Biol. 94, 483-
651        512.

652    31. Sugimoto, H., Mundel, T. M., Kieran, M. W., Kalluri, R., 2006. Identification of fibroblast
653        heterogeneity in the tumor microenvironment. Cancer Biol. Ther. 5, 1640-1646.

654    32. Treloar, K. K., Simpson, M.J., 2013. Sensitivity of edge detection methods for quantifying
655        cell migration assays. PLoS ONE. 8, e67389.

656    33. Treloar, K. K., Simpson, M. J., Haridas, P., Manton, K. J., Leavesley, D. I., McElwain, D.
657        L. S., Baker, R. E., 2013. Multiple types of data are required to identify the mechanisms
658        influencing the spatial expansion of melanoma cell colonies. BMC Syst. Biol. 7,137.

659    34. Treloar, K. K., Simpson, M. J., McElwain, D. L. S., Baker, R. E., 2014a. Are *in vitro*
660        estimates of cell diffusivity and cell proliferation rate sensitive to assay geometry? J.
661        Theor. Biol. 356, 71-84.

662    35. Treloar, K. K., Simpson, M. J., Binder, B. J., McElwain, D. L. S., and Baker, R. E., 2014b.
663        Assessing the role of spatial correlations during collective cell spreading. Sci Rep. 4, 5713.

664    36. Xie, Y., Rizzi, S. C., Dawson, R., Lynam, E., Richards, S., Leavesley, D. I., Upton, Z.,
665        2010. Development of a three-dimensional human skin equivalent wound model for
666        investigating novel wound healing therapies. Tissue Eng. PT C-Meth. 16, 1111-1123.

667    37. Ye, J., Wu, D., Wu, P., Chen, Z., Huang, J., 2014. The cancer stem cell niche: cross talk
668        between cancer stem cells and their microenvironment. Tumor Biol. 35, 3945-3951.

669    38. Zhou, L., Yang, K., Andl, T., Wickett, R. R., Zhang, Y., 2015. Perspective of targeting
670        cancer-associated fibroblasts in melanoma. J. Cancer. 6, 717-726.

671

|  | $t$=0 hours | $t$=24 hours | $t$=48 hours |
|---|---|---|---|
| Fb monoculture | a | b | c |
| SK monoculture | d | e | f |
| Co-culture 3 | g | h | i |

j
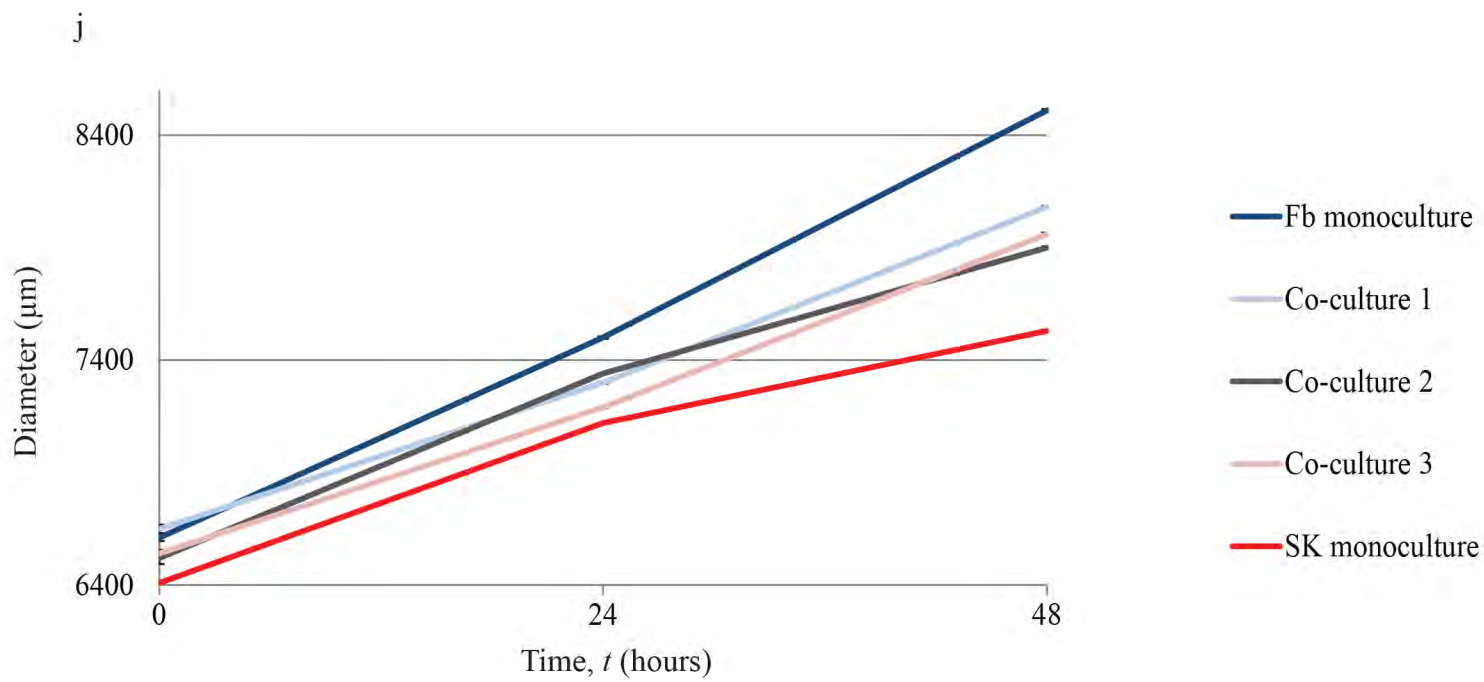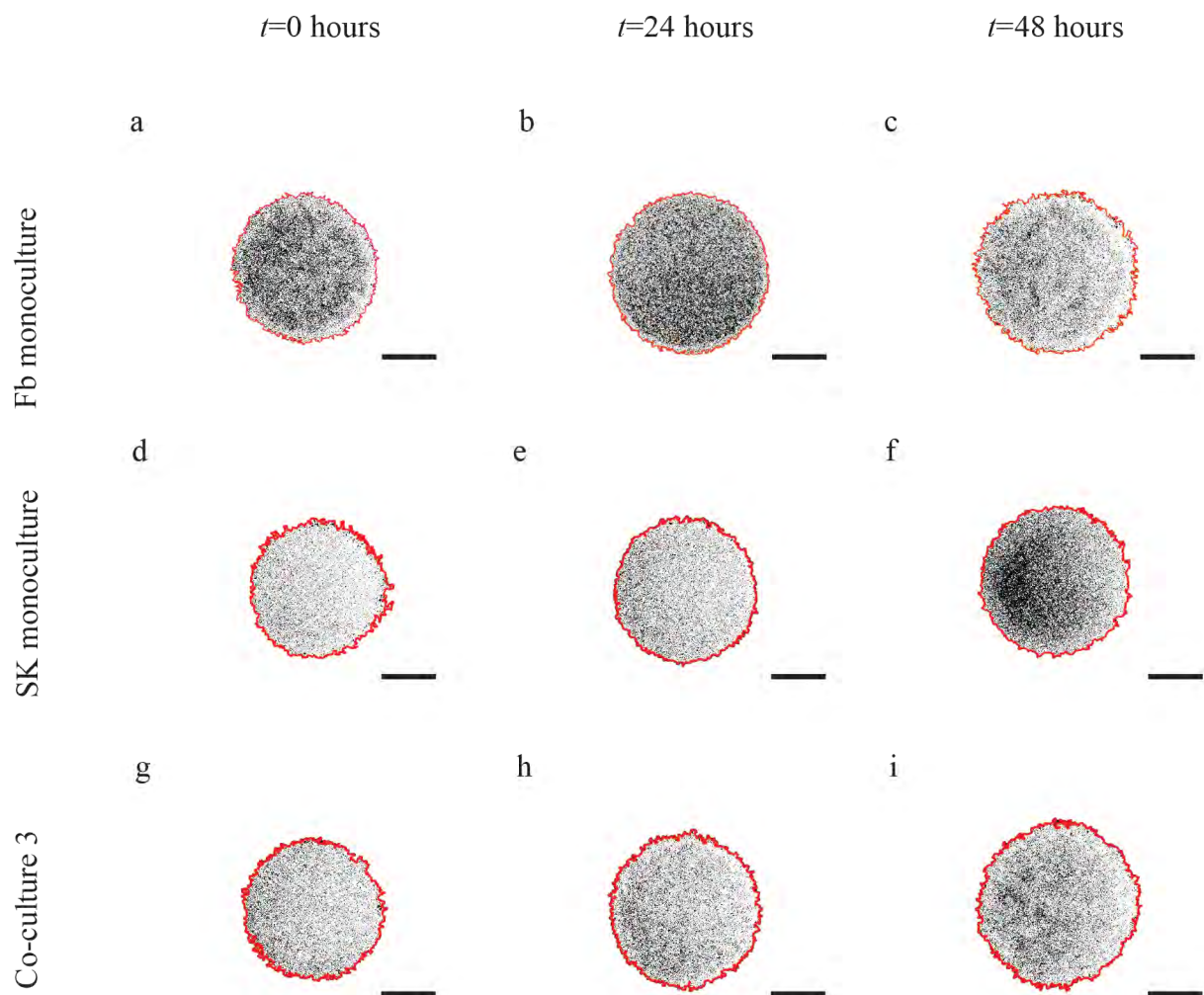
**Fig. 1.** Spatial spreading of cell populations over 48 hours. Images in (a)-(c) show monoculture barrier assays initialised with approximately 20,000 primary fibroblasts (Fb monoculture), (d)-(f) show monoculture barrier assays initialised with approximately 20,000 SK-MEL-28 melanoma cells (SK monoculture), and (g)-(i) show co-culture barrier assays initialised with approximately 10,000 SK-MEL-28 melanoma cells and approximately 10,000 primary fibroblast cells (co-culture 2). Images show the spreading of the population at $t$=0, 24 and 48 hours, as indicated. The red outline shows the position of the leading edge detected using ImageJ. Each scale bar is 3000 μm. Data in (j) show the increase in average diameter of the spreading cell populations with time (n=3). Each initial ratio of cells is shown using a different colour, as indicated. Co-culture 1 corresponds to experiments initialised with approximately 15,000 primary fibroblasts and approximately 5,000 SK-MEL-28 melanoma cells, co-culture 2 corresponds to experiments initialised with approximately 10,000 primary fibroblasts and approximately 10,000 SK-MEL-28 melanoma cells, and co-culture 3 corresponds to experiments initialised with approximately 5,000 primary fibroblasts and approximately 15,000 SK-MEL-28 melanoma cells.
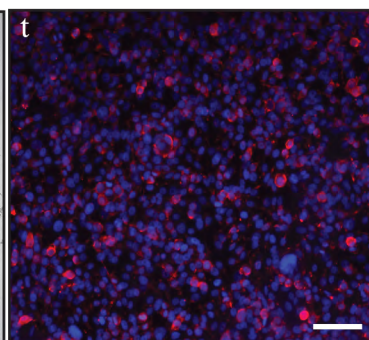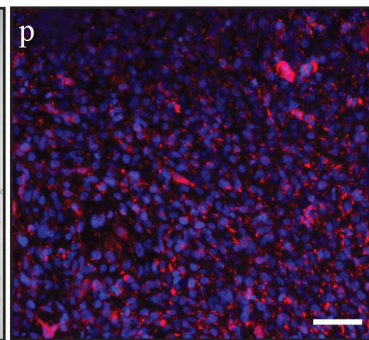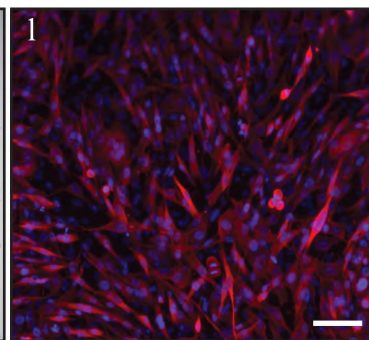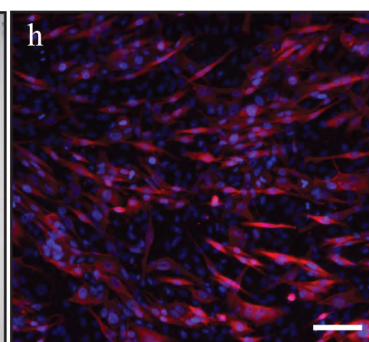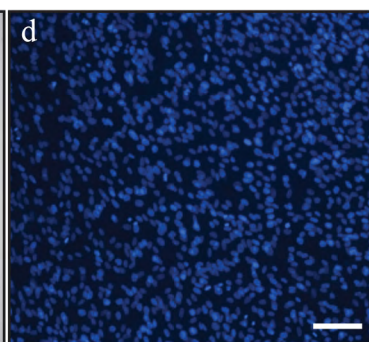
**Fig. 2.** Experimental images of spreading cell populations and corresponding immunofluorescence images to detect the composition of the co-culture assays, at $t=24$ and 48 hours. The two left-most columns of images correspond to $t=24$ hours, and the two right-most columns of images correspond to $t=48$ hours. Results in (a) and (c) correspond to Fb monoculture; (e) and (g) correspond to co-culture 1; (i) and (k) correspond to co-culture 2; (m) and (o) correspond to co-culture 3; and (q) and (s) correspond to SK monoculture, as indicated. A transect showing immunofluorescence staining is superimposed on each greyscale image, and the transect passes through the centre of each spreading population. The vertical white lines on each transect indicates the central region of the transect, and the central regions in (a), (c), (e), (g), (i), (k), (m), (o), (q) and (s) are magnified, and shown in (b), (d), (f), (h), (j), (l), (n), (p), (r) and (t), respectively. In the immunofluorescence images, all cell nuclei (Fb + SK) are stained with *dapi* (blue), whereas just the SK-MEL-28 melanoma cells (SK) are stained with *S100* (red). The scale bar in all greyscale images is 2000 µm, and the scale bar in all immunofluorescence images is 100 µm.

a

r=0

Radius, r (μm)

b

h (μm)

w (μm)

c

d

e

x10⁻³

Co-culture 2                    t=0

Density

3

2

1

0

5000                    0                    5000
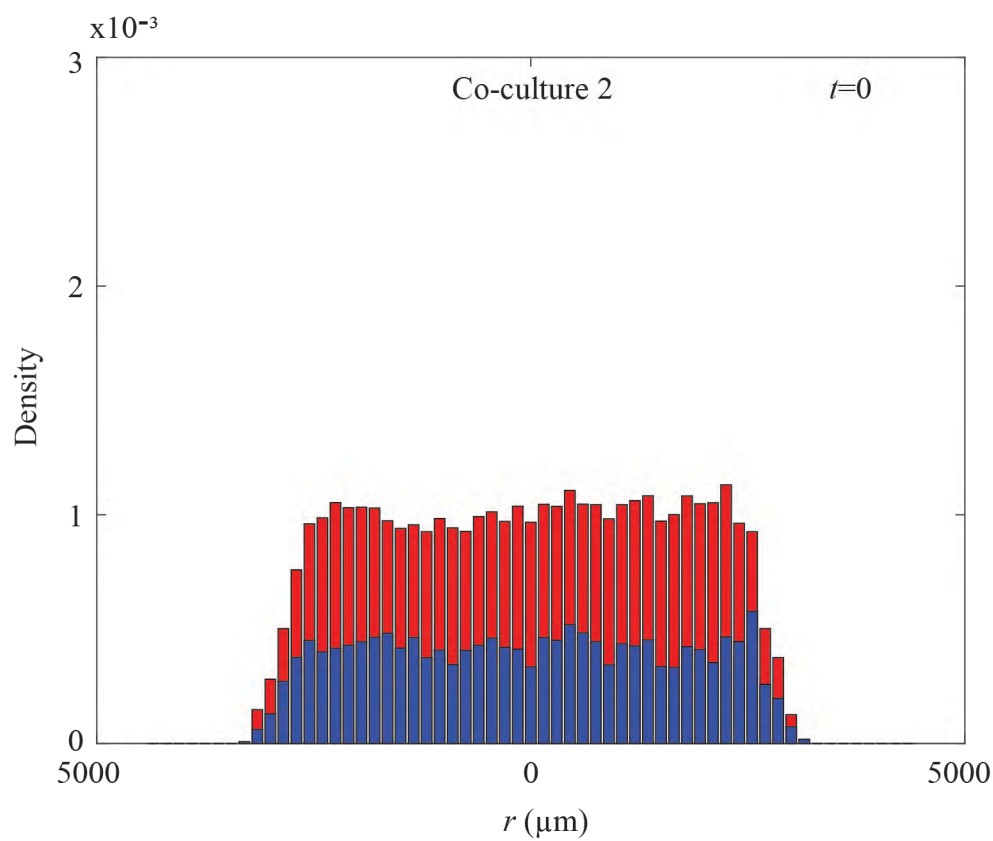
r (μm)
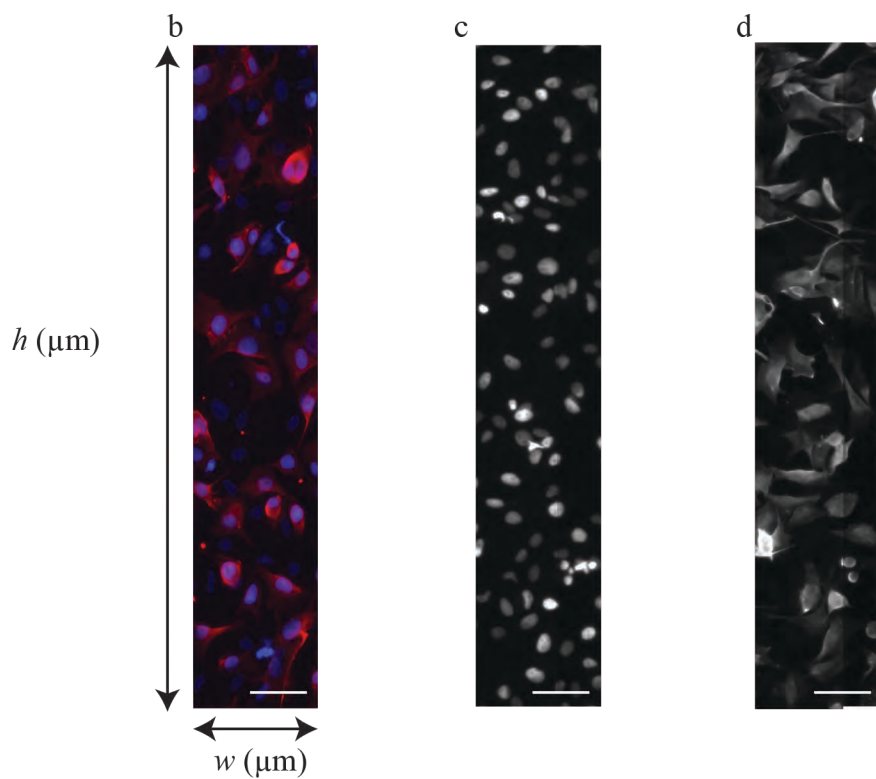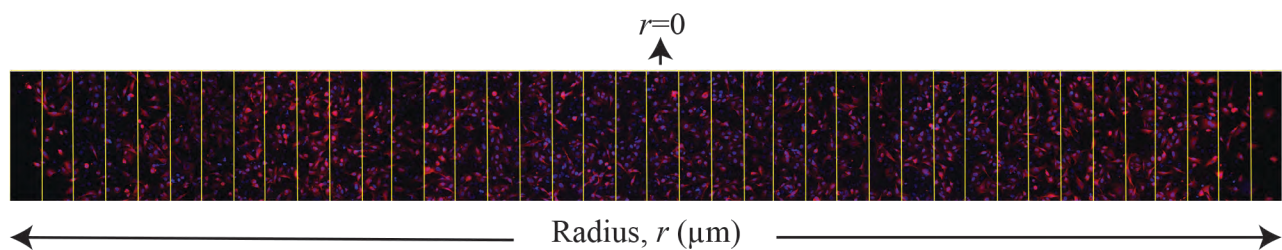
**Fig. 3.** Immunofluorescence staining identifies the spatial and temporal patterns of cell spreading in the co-culture barrier assays. (a) Example transect through the centre of a spreading population. The centre of the population corresponds to $r=0$, and the distance from the centre of the population is measured by the radial coordinate, $r>0$. Each transect is divided into many equally-spaced subregions, each of width $w=150$ μm and height $h$. The value of $w$ is constant, fixed at 150 μm in all experiments. However, the height of the subregion, $h$, varied between 622-817 μm in different experiments, but the height is constant each transect in each particular experiment. To quantify the density of cells across the transect, we count the number of cells of each type in each subregion, and divide by the area of the subregion to give an estimate of the density of each cell type, at each radial position, $r$. To count the number of cells in each subregion we use immunofluorescence staining, as shown in (b). The staining in (c) shows *dapi* staining (Fb + SK), whereas the staining in (d) shows *S100* (SK) staining. The number of primary fibroblast cells in each subregion is the difference between the total number of *dapi*-positive nuclei and the number of *S100*-positive cells in each subregion. The scale bar in (b)-(d) is 100 μm. Using these cell counts, we construct the cell density histogram, as shown in (e), illustrating the spatial variation in cell density at $t=0$ in an experiment corresponding to co-culture 2. The blue section in the histogram shows the density of primary fibroblast cells, the red section shows the density of SK-MEL-28 melanoma cells, and the total height of the histogram shows the total cell density.
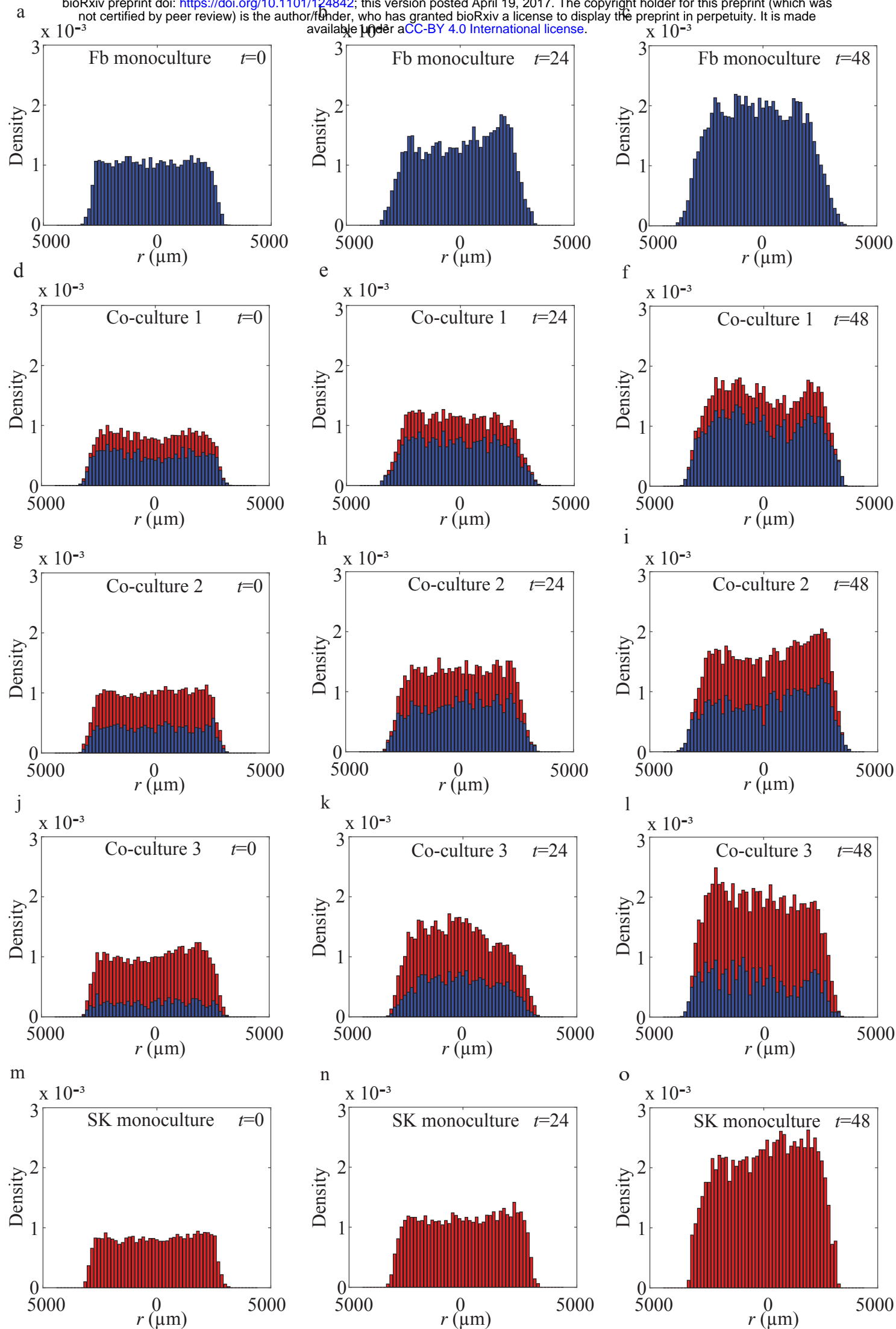
**Fig. 4.** Summary of cell density profiles. Cell density histograms for individual experiments, constructed using the technique presented in Fig. 3, are averaged across three identically prepared experimental replicates (n=3) to give a series of averaged cell density histograms. Averaged cell density histograms in (a)-(c) correspond to Fb monoculture; (d)-(f) correspond to co-culture 1; (g)-(i) correspond to co-culture 2; (j)-(l) correspond to co-culture 3; and (m)-(o) correspond to SK monoculture, at $t$=0, 24 and 48 hours, as indicated. The blue section in the histogram shows the density of primary fibroblast cells, the red section shows the density of SK-MEL-28 melanoma cells, and the total height of the histogram shows the total cell density.
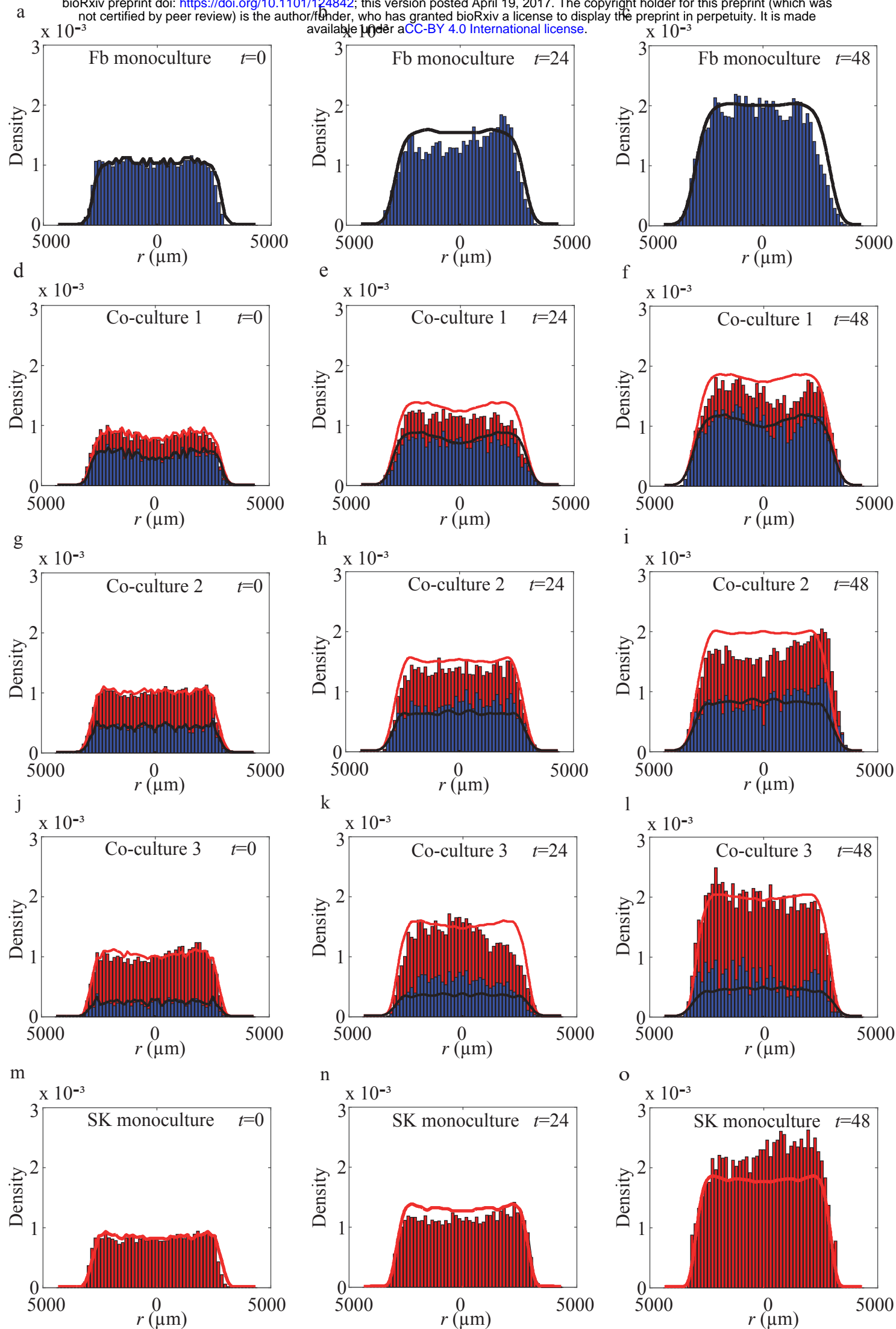
**Fig. 5.** Comparison of average cell density profiles and the solution of the mathematical model, Eq. (1)-(2). The experimental data is presented in the same format as presented in Fig. 4. All experimental data are superimposed with appropriate numerical solutions of Eq. (1)-(2), with $C_{Fb}(r,t)$ shown in black, and $S(r,t)$ shown in red, and $C_{SK}(r,t)$ is the difference between the red curve and the black curve. The initial condition for $C_{Fb}(r,0)$ and $S(r,0)$, shown in (a), (d), (g), (j) and (m), are chosen to match the observed experimental data at $t$=0. The parameters used to solve Eq. (1)-(2) are: $D_{Fb} = 1200$ μm²/hour; $D_{SK} = 170$ μm²/hour; $\lambda_{Fb} = 0.03$ hour⁻¹; $\lambda_{SK} = 0.03$ hour⁻¹ and $K = 2.8 \times 10^{-3}$ cells/μm². The equations are solved on $0 < r < 4350$ μm. Zero flux boundary conditions are implemented at $r = 0$ μm and $r = 4350$ μm. The numerical solutions of Eq. (1)-(2) are obtained with $\Delta r = 10$ μm, $\Delta t = 0.1$ hours and $\varepsilon = 1 \times 10^{-5}$.
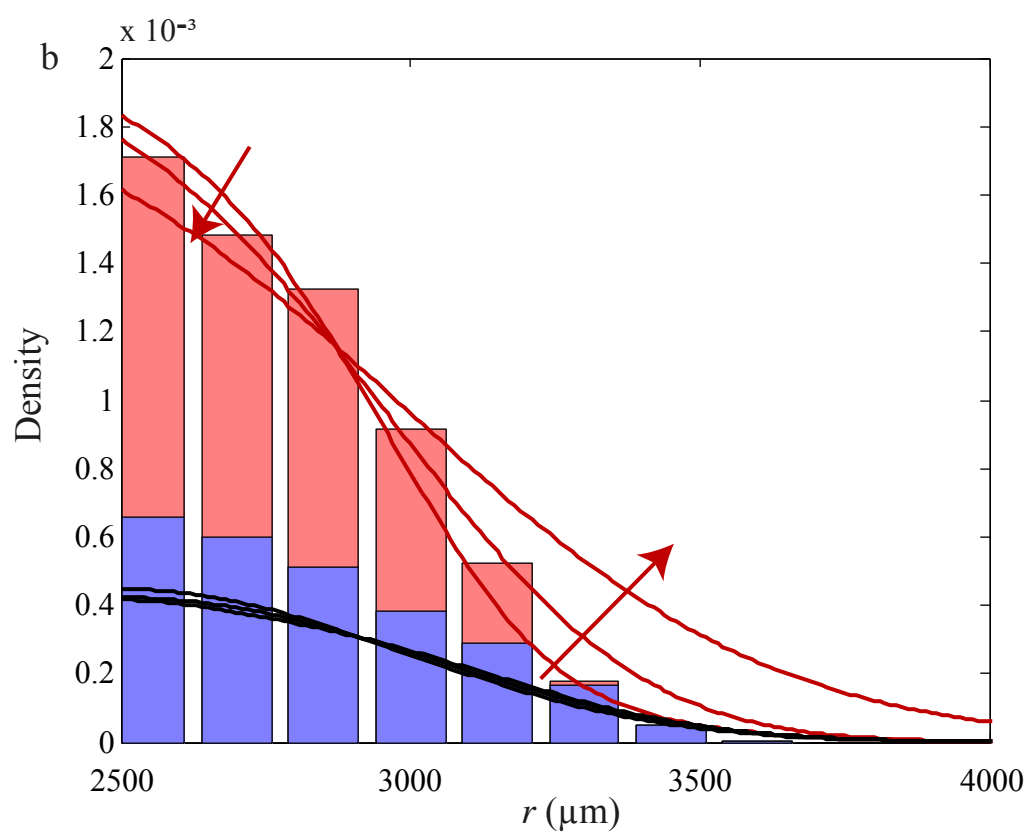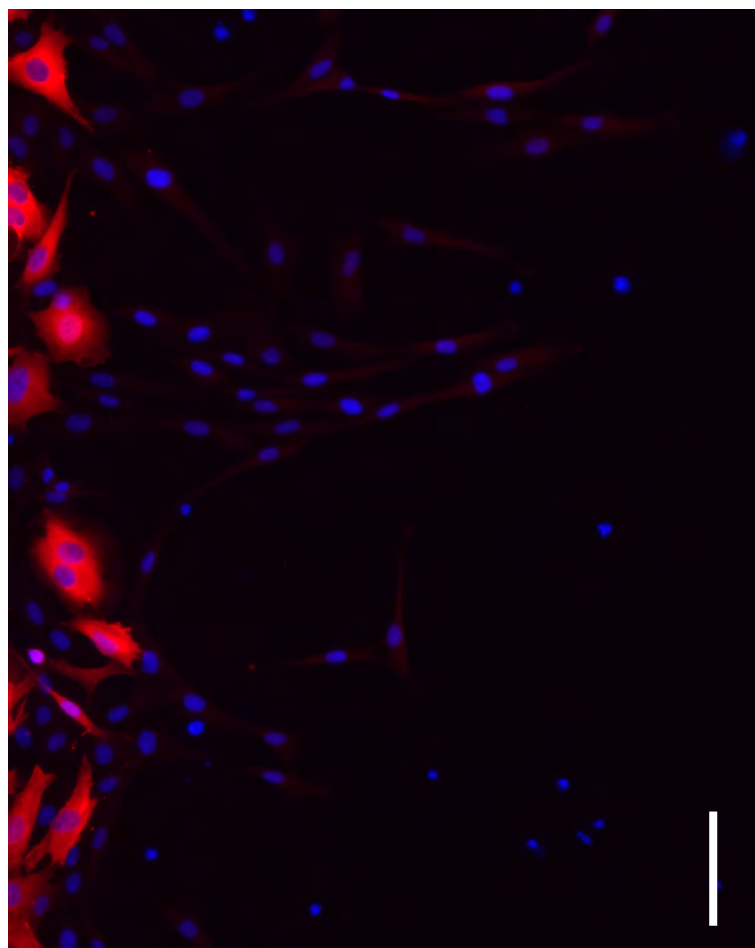
a



b

**Fig. 6.** Focussing on the leading edge of the spreading population highlights the sensitivity of

the spreading to the value of $D_{SK}$. (a) Immunofluorescence staining at the leading edge of the

spreading population in co-culture 3 showing individual fibroblast cells (blue) ahead of the SK-

MEL-28 melanoma cells (red). The scale bar is 100 μm. (b) The average experimental cell

density profile for co-culture 3 after 48 hours near the leading edge of the spreading population

is compared with three numerical solutions of Eq. (1)-(2). The solution for $C_{Fb}(r,t)$ is shown

in black, $S(r,t)$ is shown in red and $C_{SK}(r,t)$ is the difference between the red and black

curves. The parameters used to solve Eq. (1)-(2) are: $D_{Fb} = 1200$ μm²/hour; $\lambda_{Fb} = 0.03$ /hour;

$\lambda_{SK} = 0.03$ /hour and $K = 2.8 \times 10^{-3}$ cells/μm² for all three profiles, while the value of $D_{SK}$

includes 170, 850 and 3400 μm²/hour with the arrows showing the direction of increasing $D_{SK}$

. The equations are solved on $0 < r < 4350$ μm, but the profiles are shown only at the leading

edge where $2500 < r < 4000$ μm. The numerical solutions of Eq. (1)-(2) are obtained with

$\Delta r = 10$ □m, $\Delta t = 0.1$ hours and $\varepsilon = 1 \times 10^{-5}$.